Probing the Photochemical Funnel of a Retinal Chromophore Model via Zero-Point Energy Sampling Semiclassical Dynamics

Oliver Weingart,[†] Annapaola Migani,[‡] Massimo Olivucci,[‡,§] Michael A. Robb,*[,||] Volker Buss,[†] and Patricia Hunt[⊥]

Fakultät für Naturwissenschaften, Universität Duisburg-Essen, Lotharstrasse 1, 47058 Duisburg, Germany, Department of Chemistry, Imperial College London, South Kensington Campus, London SW7 2AZ, U.K., Dipartimento di Chimica, Università di Siena, via Aldo Moro 2, and Centro per lo Studio dei Sistemi Complessi, Università di Siena, via Pendola 37, Siena, Italy, and Department of Chemistry, Cambridge University, Cambridge CB2 1EW, U.K.

Received: February 26, 2004

In this work, both static and dynamic aspects of the $Z \rightarrow E$ photoisomerization of the (*Z*)-pentadieniminium cation, a minimal model of retinal (the chromophore of rhodopsin proteins), are investigated on the basis of ab initio CASSCF potential energy surfaces taking into account the full set of vibrational degrees of freedom of the molecule. In particular, the structure of the lowest lying one-dimensional cross-section of the intersection space formed by the S_1 and S_0 energy surfaces has been mapped along the $Z \rightarrow E$ isomerization of the central double bond from 0° to 180°. The evolution of a semiclassical wave packet toward the S_1/S_0 intersection seam on the basis of 70 independently calculated zero-point energy sampled trajectories has been examined. The results indicate that the photodynamics of the $Z \rightarrow E$ isomerization is controlled by a small segment of the intersection space which intercepts the excited-state reaction path. In addition to the effects of surface topography, the influence of the kinetic energy on the rate of the $Z \rightarrow E$ isomerization is also investigated.

1. Introduction

The computational investigation of the mechanism of a photochemical reaction requires the characterization of the associated photochemical funnel.[1] This is defined as the point of the excited-state reaction path where the reactant has a peak probability to decay to the ground state and initiate photoproduct formation. Consequently, the funnel structure is seen as a key mechanistic element of excited-state reactivity. In many singlet reactions the photochemical funnel has been associated with a conical intersection (CI) between the excited (S_1) and ground (S_0) state energy surfaces.[1] However, conical intersections are not isolated points of the *n*-dimensional potential energy surface (*n* being the number of vibrational degrees of freedom) but belong to a maximally $(n - 2)$-dimensional set of intersection points called intersection space.[2] This fact raises the fundamental problem of assessing if the photochemical funnel may indeed be associated with a single conical intersection structure or if the probability of decay is more homogeneously distributed along a finite segment (i.e., a subset) of the intersection space. In the last case it is an intersection space segment that represents the mechanistic entity driving the decay, and this is expected to have a substantial impact on properties such as the reaction time scale and quantum yield.

Excited-state reaction paths are defined as minimum energy paths (MEPs) computed in mass-weighted coordinates.[3] When the reaction is barrierless, these correspond to single steepest descent paths starting at the Franck−Condon point.[4,5] Recently, the mapping of different excited-state reaction paths has shown that, in several cases, such paths do not end up at the lowest energy point of the intersection space (as often assumed[1]) but at a structurally and energetically different conical intersection,[6−8] and this is the point taken as the photochemical funnel in mechanistic studies. The minimal model of the retinal chromophore of rhodopsin (the human visual pigment), the (*Z*)-penta-3,5-dieniminium cation **1**, is one of these compounds.[4,8−10]

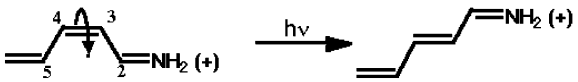

1 **2**

In a recent paper[8] we have reported the mapping of the reaction path associated with the $Z \rightarrow E$ isomerization of **1** together with the mapping of a low-lying one-dimensional cross-section of its intersection space. It was shown (see Figure 1) that the reaction path intercepts the intersection space at a 70° twisted conical intersection structure ($CI_{70°}$) and then remains substantially coincident with it up to the lowest energy intersection found in the system ($CI_{92°}$). The remaining portion of the intersection space segment *extends backward* toward the Franck−Condon point of the system ($CI_{0°} \rightarrow CI_{70°}$) and, in this region, becomes roughly parallel to the reaction path.

The documented relationship between the S_1 reaction path and $CI_{0°} \rightarrow CI_{70°} \rightarrow CI_{92°}$ intersection space segment in **1** raises some important questions. The first question is related to the nature of the photochemical funnel driving the $Z \rightarrow E$ isomerization in this chromophore. In particular, as mentioned above, one would like to assess if the conical intersection intercepted by the S_1 reaction path (i.e., $CI_{70°}$) provides an acceptable model for the photochemical funnel, or in other words if the reaction

* To whom correspondence should be addressed. E-mail: mike.robb@imperial.ac.uk.
[†] Universität Duisburg-Essen.
[‡] Dipartimento di Chimica, Università di Siena.
[§] Centro per lo Studio dei Sistemi Complessi, Università di Siena.
[||] Imperial College London.
[⊥] Cambridge University.

10.1021/jp049140b CCC: $27.50
Published on Web 05/04/2004

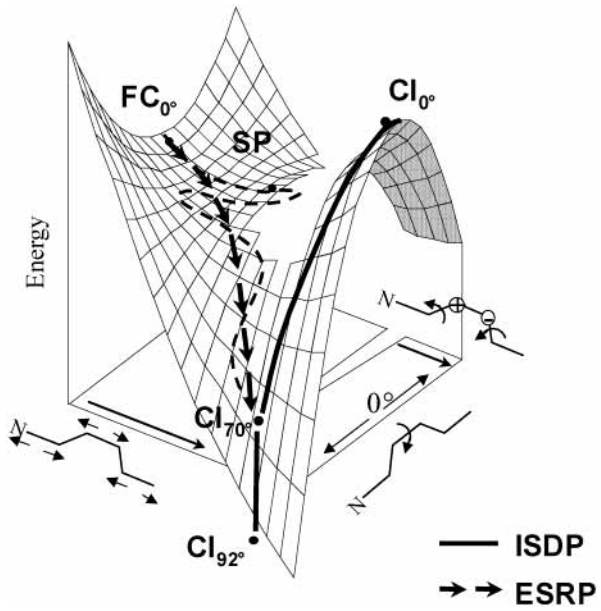

Figure 1. Schematic representation of the S_1 energy surface involved in the $Z \rightarrow E$ isomerization of **1**. The surface fault marks the structural difference between the excited-state reaction path (ESRP) and the calculated minimum energy intersection seam of the S_1 and S_0 energy surfaces (the steepest descent path within the intersection space, ISDP). SP is a planar transition structure. For simplicity the S_0 surface is not shown. The geometric coordinates correspond to the torsion about C_3-C_4 and totally symmetric stretching for the excited-state reaction path, and torsion about C_3-C_4 and conrotatory torsion about C_2-C_3/C_4-C_5 coupled with C_3/C_4 pyramidalization for ISDP. The ESRP and ISDP curves merge at $CI_{70°}$.

path defines the valley followed by the majority of the excited-state trajectories or if a significant number of trajectories escape this valley and decay at points in the intersection space far removed from $CI_{70°}$. The second question is related to the prediction of the quantum yield of the $Z \rightarrow E$ isomerization. Large deviation of the decay from the $CI_{70°}$ region and along the upper $CI_{0°} \rightarrow CI_{70°}$ segment is intuitively expected to decrease the quantum yield of the reaction since the decay would occur at structures with a torsional deformation displaced toward the reactant geometry. In contrast, deviations in the opposite direction, i.e., along the $CI_{70°} \rightarrow CI_{92°}$ segment, would, intuitively, increase the reaction quantum yield. To determine which among these different possibilities describes the behavior of the excited-state wave packet, a full statistical treatment of the dynamics is required.

Here, we compute an ensemble of trajectories that form a classical wave packet by means of ab initio CASSCF direct[11,12] semiclassical trajectory computations coupled with surface hopping[13] to provide an answer to the questions stated above. Furthermore, we extend the mapping of the intersection space. In particular we report the mapping[14] of a low-lying intersection space cross-section having a *trans*-like configuration. Our central objective in this study is to answer the question as to whether the chemistry of the $Z \rightarrow E$ isomerization can be described by the reaction path, or whether higher energy regions of the intersection space that can only be sampled by molecular dynamics become important.

Despite the differences[15] between the S_1 energy surface structure of realistic retinal chromophore models and that of our minimal model, **1** provides the only system where the relaxation between the excited-state reaction path and the dynamics of a semiclassical wave packet can be tested at the ab initio CASSCF level of theory. Our results demonstrate that the previously mapped low-lying intersection space cross-section extends well beyond 92° up to 180° twisting. (A discussion about the relationship between the $CI_{180°} \rightarrow CI_{92°}$ intersection space segment and the $FC_{180°} \rightarrow CI_{92°}$ reaction path describing the S_1 $E \rightarrow Z$ photoisomerization of **2** can be found in the Supporting Information.) This "*trans*" seam is energetically accessible relative to the Franck−Condon point of **1** ($FC_{0°}$) and therefore must be included in a complete model study of the $Z \rightarrow E$ photoisomerization of **1**.

Next we compute and analyze a set of 70 S_1 trajectories generated via zero-point energy sampling[16] applied to the reactant **1**. Remarkably, our trajectory analysis indicates the following: (i) The decay point assigned only on the basis of the excited-state reaction path (i.e., a 70° twisted conical intersection) corresponds to the region where one has the highest probability of decay of a semiclassical trajectory. (ii) It is also demonstrated that the decay in this rather "early" region (i.e., where the twisting angle is closer to that of the reactant than to that of the product) does not preclude the achievement of high quantum yields of $Z \rightarrow E$ isomerization. Indeed, our simulation predicts an 80% quantum yield for gas-phase **1**. A discussion of the structural and dynamical factors that account for (i) and (ii) is given in section 3.2.

These results support the idea that the majority of the S_1 trajectories follow quite closely the reaction path and hop in the region around the $CI_{70°}$ conical intersection. The essential point that emerges from these simulations is that for the case under investigation the topography of the S_1 surface controls the dynamical behavior in a simple classical way.

2. Computational Methods

The ground and first excited-state potential energy surfaces, gradient, and force constants were computed with the CASSCF method as implemented in the GAUSSIAN[17] series of programs. For the trajectory calculations a development version of the GAUSSIAN99 set of routines[18] was used. The active space consists of the six π-electrons distributed in the six π-orbitals. In all the results presented here a 6-31G* basis set was used. In the excited-state reaction path mapping, the S_1 and S_0 energies were computed at the two-root state-average (0.5 weight) level to ensure the convergence of the CASSCF wave function only when the two surfaces were close in energy. In the intersection space mapping and for the whole duration of the trajectory computation, we used equally weighted state-averaged wave functions for the ground and excited states.

2.1. Computation of Excited-State Reaction Paths and Steepest Descent Paths within the Intersection Space. The entire intersection space cross-section of **1** discussed below consists of two segments (see Figure 2), $CI_{0°} \rightarrow CI_{92°}$ and $CI_{180°} \rightarrow CI_{92°}$, having a *cis*-like and a *trans*-like configuration, respectively. In this work the $CI_{180°} \rightarrow CI_{92°}$ one-dimensional cross-section of the intersection space is computed in terms of a steepest descent path within the intersection space (ISDP) using the same methodology previously employed to map the $CI_{0°} \rightarrow CI_{92°}$ intersection space part.[14] This method can be described as a combination of the intrinsic relaxation direction (IRD) method for finding local steepest descent directions from a nonstationary point[19] and of the conical intersection optimization method for locating conical intersections as energy minima within the intersection space.[20] The details of this methodology are given in refs 8 and 14.

It is apparent that a steepest descent line within an intersection space is characterized by the choice of the starting point (i.e., the origin of the steepest descent path) since this is not

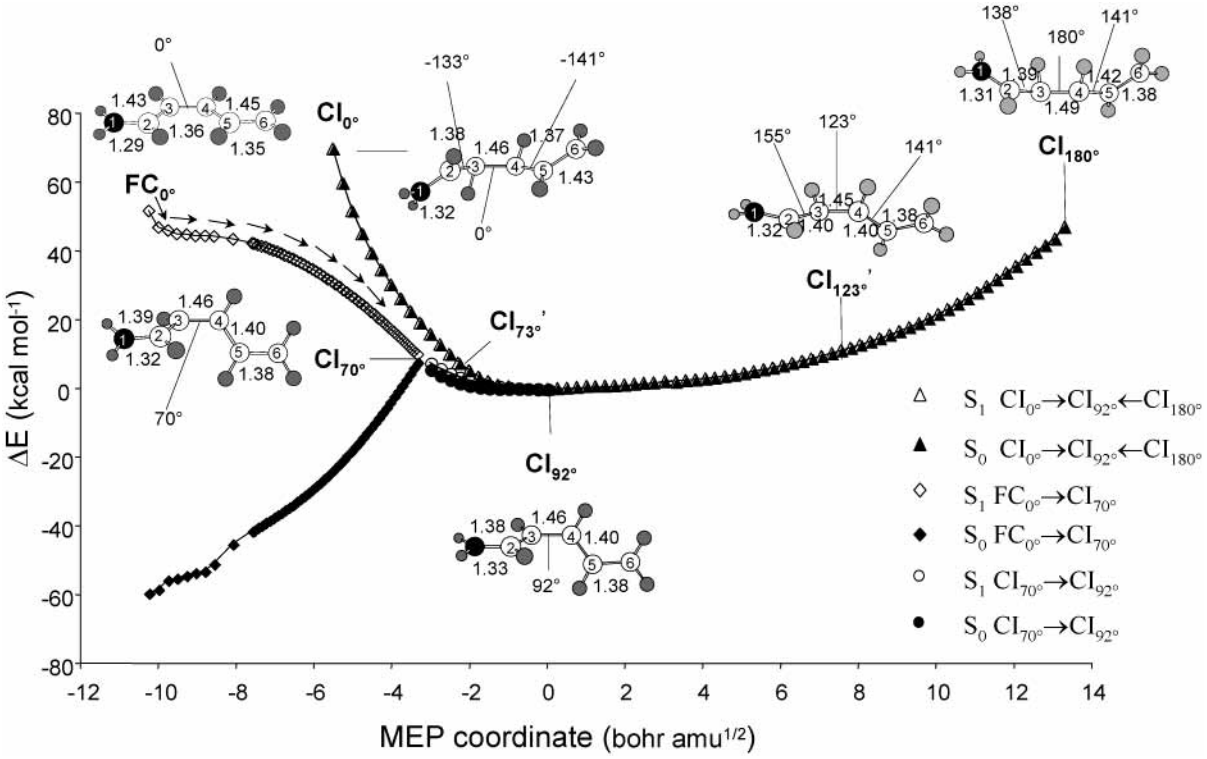

Figure 2. Energy profiles along the computed reaction path ($FC_{0°} \rightarrow CI_{70°}$) and intersection space cross-section ($CI_{0°} \rightarrow CI_{92°} \leftarrow CI_{180°}$) for the S_1 $Z \rightarrow E$ isomerization of **1**. The reaction path ($FC_{0°} \rightarrow CI_{70°}$) and the intersection space cross-section ($CI_{0°} \rightarrow CI_{92}$) data are from ref 8. The structural parameters are in angstroms and degrees.

univocally determined as in the case of reaction path calculations. For the $Z \rightarrow E$ photoisomerization of **1** the most important geometrical parameter is represented by the central bond torsion spanning the 0−180° range. A meaningful choice for the reference points of the *cis* and *trans* segments of the seam would correspond to the minimal energy intersection points in which the $C_2-C_3-C_4-C_5$ dihedral angles are 0° and 180°, respectively. The most obvious approach to locate these two points would be that of using the gradient-driven conical intersection optimization method[3,20] in which the $C_2-C_3-C_4-C_5$ torsion angle is constrained to 0° (180°) and the rest of the geometrical parameters are optimized to minimize the energy. While this approach would guarantee that the computed intersection point is the lowest energy one subject to the imposed constraint, the conical intersection optimization procedure fails to converge at $FC_{0°}$ (see ref 8 for a discussion of this point). For this reason we have used a more approximate procedure. We have performed a series of constrained geometry optimizations starting at the optimized lowest energy conical intersection point $CI_{92°}$ in which the $C_2-C_3-C_4-C_5$ dihedral angle value is fixed and smoothly augmented from 92° to 180° by minimizing the S_1-S_0 gradient difference. In each step the structure optimized in the previous step is taken as a guess geometry, with the torsional angle further augmented by 5−15°. While this procedure yields a low-lying $CI_{180°}$, the strategy does not fully guarantee that the located structure corresponds to the lowest energy conical intersection with a 180° $C_2-C_3-C_4-C_5$ torsion.

As mentioned above, the S_1 reaction path starting from the Franck−Condon region of **2** ($FC_{180°}$) and describing the $E \rightarrow Z$ photoisomerization has also been mapped using the same strategy. A discussion of the results of this computation and details on the location of $CI_{180°}$ and $CI_{0°}$ are included in the Supporting Information to this paper.

2.2. Trajectory Computation. For the semiclassical trajectory calculations a set of positions and momenta (initial conditions) must first be generated to represent the nuclear wave packet. The sampling was carried out on the ground-state surface. Thus, the ground-state minimum of **1** was optimized, and the second derivatives of the energy with respect to the coordinates (i.e., the frequencies) were calculated. The ground-state vibrational modes were sampled[16] at 0 K, and the resulting geometries and velocities were used as starting conditions for the trajectory calculations.

The trajectory calculations were started in the first electronically excited state simulating the Franck−Condon excitation of the molecule from the ground-state zero-point energy valley to the excited-state S_1 surface. Trajectories were calculated "on the fly" [11,12] by solving Newton's equations of motion for the nuclei in the full space of coordinates. We use a trust region dynamics scheme that approximates the potential energy surfaces to second order and apply local corrections to fifth order when propagating the next step in the simulation.[11,12,21] In this trust radius scheme the trajectory time step is variable and depends on the local surface topology. Typical values are between 0.5 and 1.5 fs. The nonadiabatic surface hop[13] is determined by propagating the solutions of the time-dependent electronic Schrödinger equation in concert with nuclear propagation. The population of the two states, obtained from the projection of the time-dependent wave function on the adiabatic basis states, is used to determine when the surface hop occurs.[22] After a hop the energy is conserved by correcting the momentum in the direction parallel to the derivative coupling vector.

A set of 70 independently initialized trajectories was followed for up to 160 fs, or at least up to a point where a decision could be made whether the trajectory would lead to the *trans* (*E*) product or back to the *cis* (*Z*) educt. The decision is based on the development of the central torsion angle when after a surface hop the system has left the coupling region. This irreversible "leaving of the hopping region" corresponds to an energy criterion: only when the potential energy of S_0 has dropped by

a significant amount relative to that of S_1—between 15 and 20 kcal mol^{-1}—do we consider the probability of it returning to S_1 as nil. From the direction which the trajectory has taken after the surface hop, it is then possible to decide whether the final destination will be the *trans* or the *cis* product. We have carefully reviewed each of the trajectories and found the classification confirmed: in the trajectories designated as "*trans*" the trajectory had moved irreversibly out of the hopping region toward an increased twist angle; in the trajectories designated as "*cis*" the movement was out of the hopping region toward a decreased twisting angle. In a different study we have shown that our number of trajectories, 70, is sufficient to obtain a converged result.[23]

3. Results and Discussion

3.1. Intersection Space. In Figure 2 we report the full structure of the computed low-lying one-dimensional cross-section of the intersection space ($CI_{0°} \rightarrow CI_{92°} \leftarrow CI_{180°}$) and show its relationship with the previously documented[8] $FC_{0°} \rightarrow CI_{70°}$ S_1 reaction path describing the excited-state $Z \rightarrow E$ isomerization of **1**. In section 3.2 this potential energy data will be employed as a basis for the discussion and analysis of the trajectories describing the photoisomerization dynamics of the same chromophore. The energies of the critical points discussed in the text are collected in Table 1.

The $CI_{0°}$ and $CI_{180°}$ conical intersections are found to lie 18 kcal mol^{-1} above and 5 kcal mol^{-1} below the FC point of **1**, respectively. These two conical intersection points have important common structural features as well as some structural differences. As can be seen in Figure 2, both structures have a large C_3 and a less pronounced C_4 pyramidalization character (325° compared to 340°). Further, they have a large conrotatory torsion about the C_3-C_4 and C_4-C_5 bonds. As previously reported,[8] the pyramidalization and conrotatory torsion coordinates characterize the conical intersections where the central torsion is smaller or larger than 90°. *Since the S_1 reaction path coordinate does not involve any contribution of these molecular modes, one can conclude that the reaction path and the intersection space seam span rather different regions of the configuration space until they meet at $CI_{70°}$*. In the next section we will show, by means of a comparative analysis of the intersection space and dynamics data, that the pyramidalization coordinate (dominated by pyramidalization at C_3) is responsible for the degeneracy along the $CI_{0°} \rightarrow CI_{92°} \leftarrow CI_{180°}$ intersection seam. The $CI_{0°}$ and $CI_{180°}$ conical intersections and the minimal energy conical intersection, $CI_{92°}$, have quite similar skeletal distances. However, at $CI_{0°}$ the C_3-C_4 and C_4-C_5 bond distances are inverted relative to those at $CI_{92°}$. Further, the central bond distance C_3-C_4 is slightly longer in the $CI_{180°}$ intersection—1.49 Å compared to 1.46 Å in $CI_{92°}$ and $CI_{0°}$. These bond length discrepancies account for the large difference in energy of the two conical intersection starting points relative to $FC_{0°}$. Of course, as mentioned in section 2.1, we cannot exclude that this difference is overestimated since lower energy structures that we fail to locate may exist. (Notice also that the $CI_{180°} \rightarrow CI_{92°}$ segment is lower in energy than the $CI_{0°} \rightarrow CI_{92°}$ segment. In the Supporting Information to this paper, this topic is discussed.)

The data reported in Figure 2 provide the basis for the discussion of the dynamics in the following section. We show the following: (i) The reaction path describing the excited-state $Z \rightarrow E$ isomerization of **1** leads directly toward a 70° twisted conical intersection point, $CI_{70°}$, located 7 kcal mol^{-1} above the minimal energy conical intersection point, $CI_{92°}$. (ii) $CI_{70°}$ is essentially coincident with the $CI_{73°}'$ point located along the $CI_{0°} \rightarrow CI_{92°}$ segment of the intersection space. As previously reported,[8] the "distance" between the $Z \rightarrow E$ excited-state reaction path and the $CI_{0°} \rightarrow CI_{92°}$ intersection seam coordinates decreases monotonically up to the $CI_{70°}$ region where these paths merge (see Figure 1). (iii) The intersection space extends for a broad range of $C_2-C_3-C_4-C_5$ dihedral angles (from 0° to 180°), and the majority of this space is energetically accessible since it lies almost completely below the $FC_{0°}$ point.

TABLE 1: CASSCF 6-31G* Absolute (E) and Relative (ΔE)[a] Energies for the (Z)-Penta-3,5-dieniminium Cation 1

structure	state	E (au)	ΔE (kcal mol^{-1})
$FC_{0°}$[b,c]	S_0	(−248.26236)[d]	
	S_1	(−248.07879)[d]	
	S_0	−248.24918[e]	−59.43
	S_1	−248.07206[e]	51.72
$CI_{70°}$[c]	S_0	−248.1456[e]	5.56
	S_1	−248.14278[e]	7.34
$CI_{92°}$[c]	S_0	−248.15455[e]	−0.05
	S_1	−248.15447[e]	0.00
$CI_{0°}$[c]	S_0	−248.04326[e]	69.79
	S_1	−248.04302[e]	69.94
$CI_{73°}$[c]	S_0	−248.14250[e]	7.56
	S_1	−248.14247[e]	7.53
$CI_{180°}$	S_0	−248.07942[e]	47.09
	S_1	−248.07939[e]	47.11
$CI_{123°}$	S_0	−248.13691[e]	11.02
	S_1	−248.13690[e]	11.03
A	S_0	−248.05785[e]	60.63
	S_1	−248.05364[e]	63.27
A′	S_0	−248.09024[e]	40.30
	S_1	−248.08723[e]	42.19
A″	S_0	−248.10418[e]	31.56
	S_1	−248.09769[e]	35.63
B	S_0	−248.09935[e]	34.59
	S_1	−248.08638[e]	42.73
B′	S_0	−248.11728[e]	23.34
	S_1	−248.11094[e]	27.32
B″	S_0	−248.12208[e]	20.33
	S_1	−248.11397[e]	25.41
C	S_0	−248.07438[e]	50.26
	S_1	−248.05618[e]	61.68
	S_0	(−248.09693)[d]	
$HM_{C\rightarrow Z}$[f]	S_0	(−248.12500)[d]	
$HM_{C\rightarrow E}$[f]	S_0	(−248.15922)[d]	
D	S_1	−248.07917[e]	47.25
	S_0	−248.07500[e]	49.89
	S_0	(−248.09819)[d]	
$HM_{D\rightarrow Z}$[f]	S_0	(−248.13000)[d]	
$HM_{D\rightarrow E}$[f]	S_0	(−248.16890)[d]	

[a] Energies relative to the lowest energy conical intersection point, $CI_{92°}$. [b] The energies of the first five points along the $FC_{0°} \rightarrow CI_{92°}$ photoisomerization minimum energy path have been scaled, by means of state-average single-point energy calculations, to match the energies of all remaining points in Figure 2 computed at the state-average CASSCF level. [c] Data from ref 8. [d] Single-state energies (in parentheses). [e] State average energies. [f] HM indicates the starting point of the MEP on the ground-state surface shown in Figure 8.

The existence of a well-defined channel on the S_1 surface leading directly to the $CI_{70°}$ intersection implies an increased importance of this point relative to that of other points of the intersection space lying "ahead" of or "after" $CI_{70°}$. Thus, potentially this region constitutes the major $S_1 \rightarrow S_0$ decay channel driving the $Z \rightarrow E$ photoisomerization of **1**. In the following section we validate this conjecture via trajectory computations.

3.2. Photoisomerization Dynamics. In this section we investigate the dynamics of a wave packet emulated by an ensemble of 70 semiclassical trajectories generated by zero-point energy sampling. The dynamics of the reverse $E \rightarrow Z$ photoisomerization of **2**, which may be related to the $E \rightarrow Z$

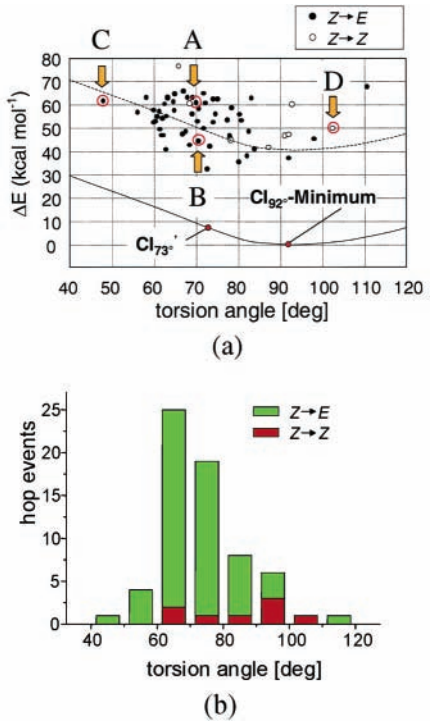

Figure 3. (a) S_1 energy distribution at the hop geometries as a function of the $C_3-C_4-C_5-C_6$ torsion. Data refer to the trajectories that hop within the simulation time (65 over 70). The energy of the intersection space segment (0−120° range) relevant to the excited-state dynamics of **1** is also shown as a single line as a function of the $C_3-C_4-C_5-C_6$ torsion. S_1 energies are relative to the minimal energy intersection point $CI_{92°}$. Full circles denote formation of *E* product, and open circles denote regeneration of *Z* educt. A higher energy one-dimensional cross-section of the IS is schematically indicated with a dashed line. The ground-state relaxation of the hop structures at points A−D is discussed in detail in section 3.3. (b) Distribution of the $C_3-C_4-C_5-C_6$ torsion of the hop geometries. The figure also shows the total number of hops in a set of 65 trajectories that lead to the *Z* educt (dark gray) or *E* product (light gray) as a function of the $C_3-C_4-C_5-C_6$ torsion.

photoisomerization of retinal PSB in bacteriorhodopsin, will not be investigated here.

All the trajectories but five in our simulation led to a point on the S_0/S_1 conical intersection at which they hopped within the simulation time. Figure 3a shows the distribution of the S_1 potential energy of the hop geometries as a function of the $C_2-C_3-C_4-C_5$ torsion. The fact that the decay occurs for a broad range of dihedral angles (between 50° and 110°) indicates that the trajectories are sampling a relatively large portion of the $CI_{0°} \rightarrow CI_{92°} \leftarrow CI_{180°}$ intersection seam shown in Figure 2. The remaining part of the intersection space that is not sampled does not play any role in the photoisomerization dynamics of **1**. Noticeable is that the gradient difference and the derivative coupling vector at the decay points show essentially skeletal deformations and coupled pyramidalizations rather than torsional motion. A dense cluster of points in the 60−80° range shows that hopping to S_0 essentially takes place in a small region of the intersection space between 60° and 80°. The distribution of the twisting angle is also shown in Figure 3b. The diagram shows that there is a maximum around 70°. Thus, our dynamics simulations indicate that *the statistically relevant region of the intersection space (i.e., the one accessed upon excitation of* ***1****) is centered on a dihedral angle of ~70° in complete agreement with predictions made on the basis of the Z → E reaction path calculations shown in Figure 2*.

To allow for a more detailed comparison of the structure and energy of the hopping and low-lying points in the intersection space, the energy profile of a 40° → 120° segment of the computed intersection space has been reported in Figure 3a. The plot shows that all hopping points are located within 20−50 kcal mol^{-1} above the corresponding intersection space structures (i.e., the one with the same torsional deformation). The initial conditions for the trajectory computations are obtained by converting the *ground-state* zero-point vibrational energy into *excited-state* initial coordinates and momenta. Thus, the majority of the trajectories contain an initial excess (kinetic and/or potential) energy with respect to the Franck−Condon point. In these conditions, "parallel" intersection space cross-sections of higher energy (but belonging to the same $(n-2)$-dimensional set) become accessible (see the dashed energy profile in Figure 3a). This means that, at decay, the conical intersection structure reached by each trajectory must be distorted relative to that of the corresponding conical intersection point lying along our low-lying intersection space cross-section. The nature of this distortion is analyzed in Figure 4 for four significant geometrical parameters. The mean C_3-C_4 and C_4-C_5 distances are 1.488 and 1.431 Å (hopping geometries) compared to 1.454 and 1.395 Å (points in the intersection space) and are therefore expanded with respect to the low-lying intersection space points (the values for the intersection space points are averages over the 48° → 111° range). The C_3-H bond (Figure 4c) shows a different behavior and is either lengthened or shorthened with maximum and minimum values of 1.245 and 0.960 Å, respectively. Finally, pyramidalization at the C_3 center (Figure 4d) expressed by the $H-C_3-C_2-C_4$ improper torsion displays a linear correlation between the degree of pyramidalization and the twisting about the central C_3-C_4 bond. The regression line and the intersection seam curve are almost superimposed. This result is important since it shows that the hopping geometries do have the same key structural features found for the low-lying intersection space cross-section. Further, the tendency to pyramidalize increases when the torsional deformation deviates from the $C_2-C_3-C_4-C_5$ 92° reference value. A similar behavior has been reported[7,24] for ethylene, for which it has been observed that accessing the conical intersections requires a substantial distortion along the pyramidalization of one of the methylene groups from the twisted geometry.

To determine the origin of the excess potential energy associated with hopping points, we have carried out the following numerical experiment. We have considered structures A and B (circled points in Figure 3a) located 56 and 35 kcal mol^{-1} above the minimal energy conical intersection $CI_{70°}$. As shown in Figure 5, in both structures the central C_3-C_4 bond is significantly stretched, and this stretching is more pronounced in the highest energy intersection A. Another main difference is the C_3-C_4 bond in structure A and C_2-C_3 in structure B, and the CH distances, for instance, the C_4-H bond that is compressed by 0.07 Å in structure A and stretched by 0.04 Å in structure B. The A and B conical intersections have also rather different bond angles as compared to $CI_{70°}$.

To estimate the contribution of the stretching deformations to the excess potential energy, we have carried out a constrained conical intersection optimization (see section 2) starting with the A and B geometries (open and full tilted squares indicate S_1 and S_0 energies relative to that of $CI_{92°}$) and optimizing only the bond lengths. These optimizations lead to the relaxed structures A′ and B′ (open and full squares) located ca. 35 (S_1) and 20 (S_1) kcal mol^{-1} above $CI_{70°}$, respectively. This means that the stretching deformation accounts for ca. 63% and 57% of the excess energy in the high- and low-energy structures,

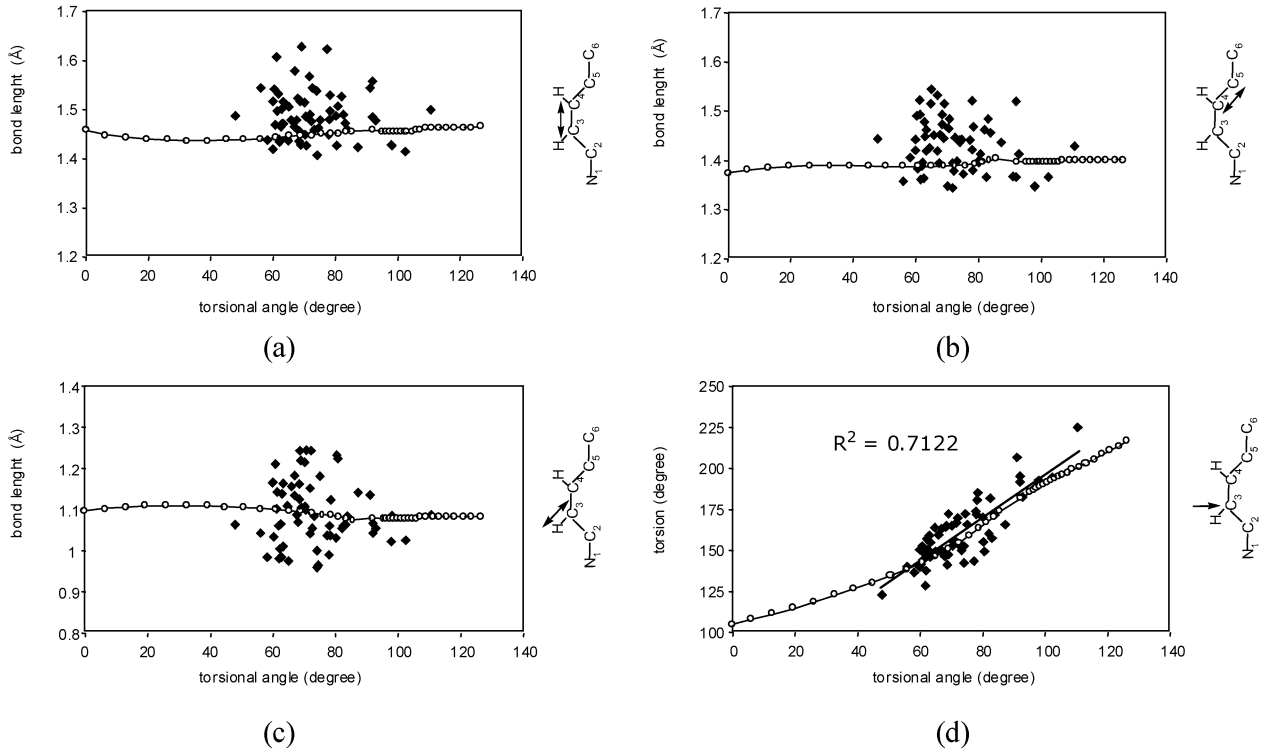

Figure 4. Comparative structural analysis between hop geometries (full tilted squares) and ISDP conical intersection structures (open circles) based on (a) C_3-C_4 bond, (b) C_4-C_5 bond (c) C_3-H bond, and (d) C_3 pyramidalization expressed by the $H-C_3-C_2-C_4$ improper torsion as a function of the isomerization angle (i.e., $C_3-C_4-C_5-C_6$ torsion). Note that a linear correlation between the C_3 pyramidalization and the isomerization angle is obtained. The square of the linear regression coefficient, R^2, is also shown.

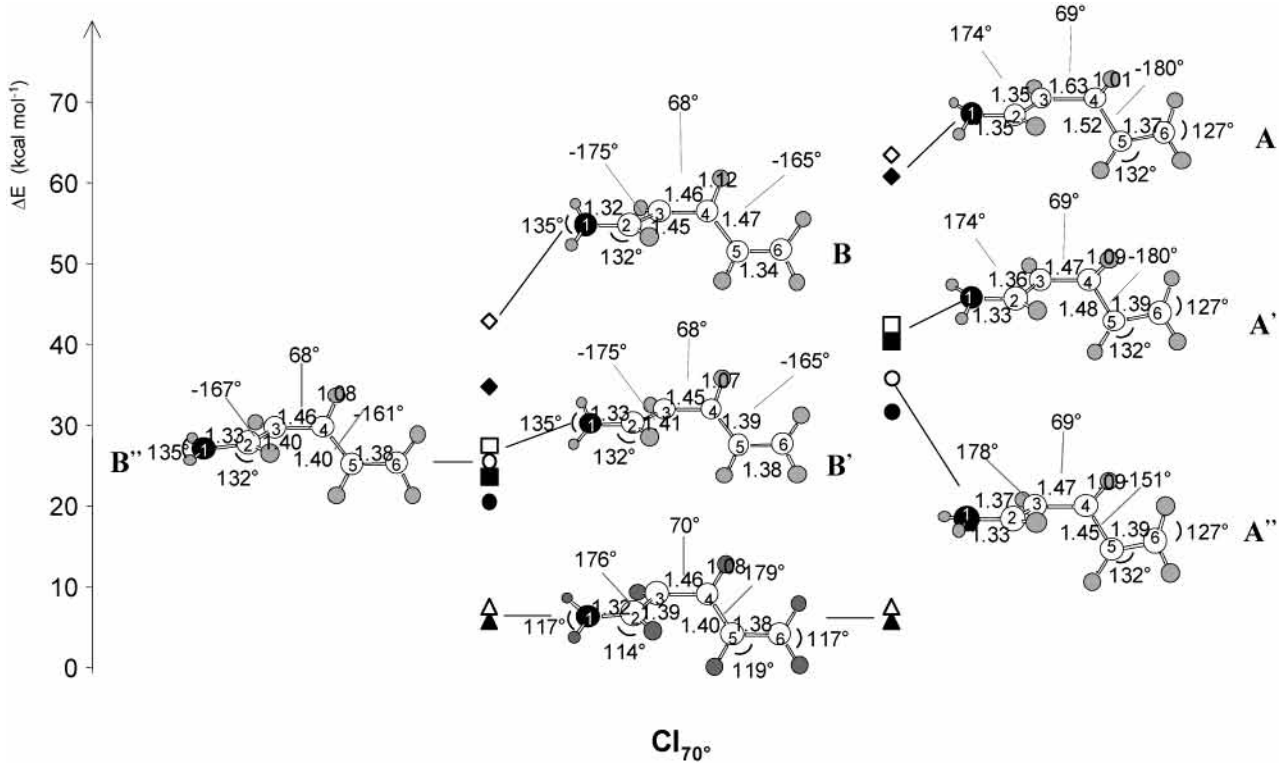

Figure 5. Estimate of the stretching, bending, and torsional potential of the hop geometries A and B in Figure 2 accomplished by means of constrained conical intersection optimizations. Relaxations of stretchings lead to A′ and B′. Relaxations of stretchings and torsions (except the reference $C_2-C_3-C_4-C_5$ dihedral angle) lead to A″ and B″. The structural parameters are in angstroms and degrees.

respectively. To evaluate the excess potential energy stored in the bending coordinates, we have carried out a second constrained CI optimization starting with A′ and B′ and optimizing the values of all stretching and dihedral angles except for the reference $C_2-C_3-C_4-C_5$ dihedral angle. This optimization leads to structures A″ and B″ (open and full circles) that are higher in energy by 28 and 18 kcal mol^{-1} compared to $CI_{70°}$. Thus, there is only very limited relaxation amounting in both cases to 5% of the total potential energy. This means that the remaining excess energy is due to bending deformations.

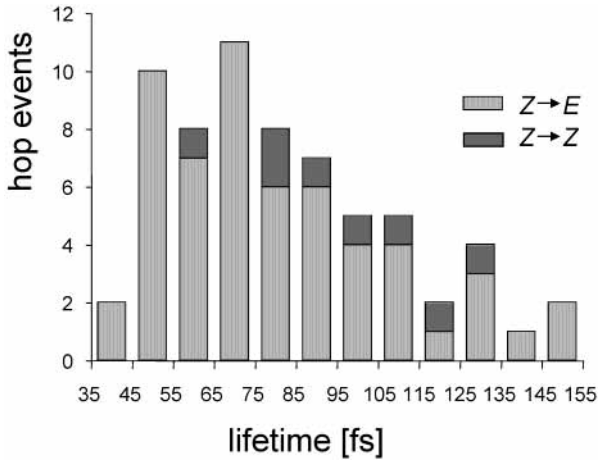

Figure 6. Distribution of the S_1 excited-state lifetimes in a set of 65 trajectories of model chromophore **1**.

3.2.1. Quantum Yield. In Figure 3a information is also given on whether the trajectory on the ground state proceeds toward the product or back to the educt. Full circles show when the *E* product is formed, and open circles denote the regeneration of the *Z* educt. Of the 70 trajectories, 57 (81%) represent successful $Z \rightarrow E$ isomerization events, 8 (11%) start twisting around the central bond but eventually return to the *Z* educt, 5 (7%) do not hop within the simulation time (not included in the diagram). In those simulations we observe the torsion of the C═N bond coupled with N-pyramidalization and strong in-plane skeletal motions, but essentially no torsion of the C═C double bond. And the S_1 and S_0 surfaces approach each other to not less than 10 kcal mol^{-1}.

These data show that the reaction is highly selective involving isomerization of the central double bond. In only two cases (3%) we observe concomitant isomerization of a different double bond. The $Z \rightarrow E$ photoisomerization reaction quantum yield of **1** predicted on the basis of the dynamic simulations is 0.81. The quantum yield of 11-*cis*-retinal-protonated Schiff base photoisomerization to *all-trans* is 25%[25] in methanol and 67%[26] in rhodopsin. Thus, the predicted 0.81 quantum yield for the photoisomerization of **1** would make our simulated vacuum isomerization one of the most efficient $Z \rightarrow E$ photoreactions observed in PSBs.

3.2.2. Reaction Time Scale. The average time taken to reach the surface-hopping region provides an estimate of the excited-state lifetime. This is ca. 79 fs, consistent with a barrierless reaction path as the presence of an excited-state barrier would slow the excited-state evolution. Figure 6 shows that 12 trajectories have short lifetimes (<50 fs), the majority of the trajectories (i.e., 39) decay with a lifetime of $50 \leq \tau \leq 100$ fs, and only 14 trajectories decay with significantly longer times (>100 fs). No correlation has been found between lifetimes and torsional angles.

3.2.3. Nature of the Surface Crossing. The nature of the surface crossing is analyzed in terms of the S_1-S_0 energy gap at hopping (Figure 7). This quantity indicates whether the decay occurs in the strict vicinity of a conical intersection point, in other words, whether the trajectory must reach the intersection space to decay. When the gap is large, the observation of a decay event implies the existence of a large electronic coupling between S_1 and S_0 in that region. We found that our trajectories have different energy gaps ranging from 1 to 13 kcal mol^{-1}. Fifteen trajectories can be classified as passing through strict conical intersections as the energy gap is $\Delta E \leq 2$ kcal mol^{-1}, 20 trajectories decay in the immediate proximity of conical intersections through regions with energy gaps between 2 and 4 kcal mol^{-1}, and the remaining 35 trajectories decay through regions with larger energy gaps ($\Delta E \leq 13$ kcal mol^{-1}). A similar distribution was reported by Warshel et al. in a recent QM/MM simulation for the photoisomerization of the retinal chromophore in bacteriorhodopsin.[27] Finally, we observe that no correlation was found to exist between the magnitude of the energy gap and type of photoproduct (*Z* versus *E*).

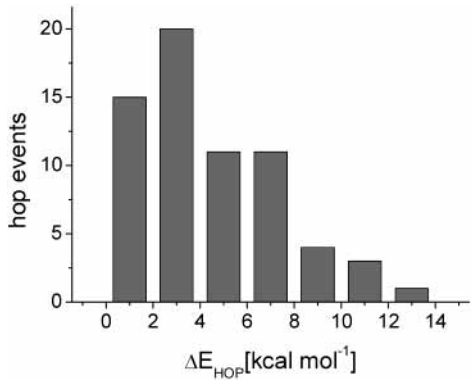

Figure 7. Distribution of S_1-S_0 energy gaps at hop geometries in a set of 65 trajectories of model chromophore **1**.

3.3. Ground-State Relaxation. In section 3.2 we have seen (see Figure 3) that trajectories that decay at small twist angles (<92°), and are therefore expected to lead to reactant reconstitution, do instead evolve toward the 180° twisted product. Similarly, it can be seen that some trajectories that lead to reconstitution of the starting material (i.e., the *Z* stereoisomer) display large $C_2-C_3-C_4-C_5$ dihedral angles at the hopping time. This type of behavior is somehow counterintuitive since one would expect intersection structures with large twisting angles to lead to photoproduct formation rather than reactant regeneration. To unveil the factors controlling the product distribution, we have investigated the geometrical structure and relaxation paths at the two "extreme" decay points marked as C and D in Figure 3a.

Trajectories starting from the decay point C without inital kinetic energy lead back to the *Z* educt, thus indicating that the relaxation path from low torsion angles is determined by the structure of the potential energy surface. This is consistent with the intuitively expected result. In the sampled dynamics the molecule does not follow the same relaxation path but successfully reaches the product valley. More detailed information about the surface topology in the vicinity of a decay point can be obtained by computing the possible relaxation directions[3,19,28] on the ground-state surface from this point and the associated minimal energy paths that lead from here to the corresponding reactant. Figure 8 shows the calculated MEPs from decay points C and D. Starting from point C (left), we have located two relaxation paths leading to the *Z* and *E* species. Both paths are extremely steep, supporting the idea that even a limited amount of properly directed kinetic energy may be enough to successfully populate either path. However, from the figure it is evident that the relaxation path leading to the *Z* species starts in the vicinity of C while the relaxation path leading to the photoproduct begins at a much larger distance and involves significant geometrical deformation, including an approximately 20° torsional deformation about the central bond and bond length changes (e.g., the C−N bond). Structurally, the reaction back to the educt is favored, and the kinetic energy component at decay must be responsible for the fact that the computed trajectory does not follow the most favorable relaxation path. In other words, when in the excited state the torsional coordinate

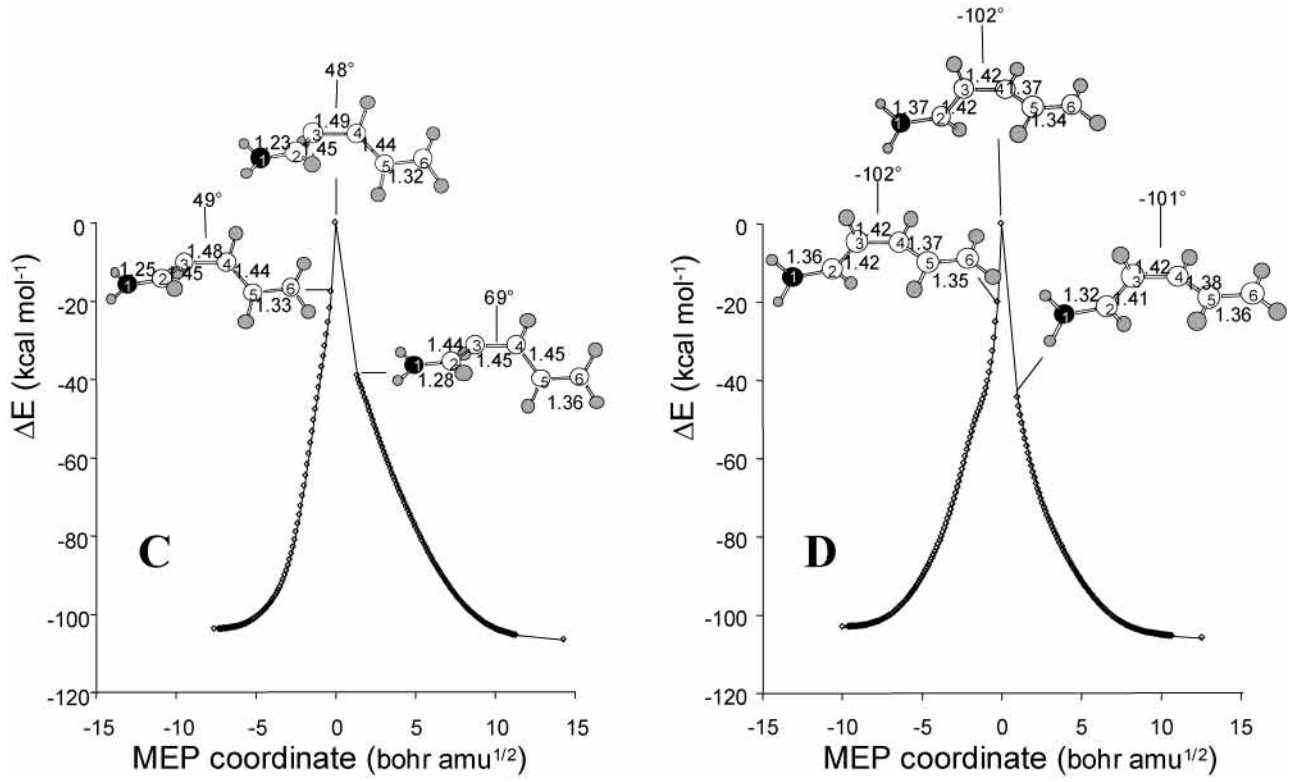

Figure 8. Structure of the S_0 potential energy surface around points C and D shown in Figure 2. The figure shows the energy profiles along the MEPs starting at C and D and leading to the ground-state *E* and *Z* minima. The structural parameters are in angstroms and degrees. Energies are relative to those of C and D.

is activated, the molecule is accelerated along this extremely steep segment of the PES. In most of the cases the torsional component gains so much momentum that even when decaying at torsional angles below 70° the motion is followed in the ground state regardless of the structure of the PES in this region.

At point D, which features a 102° torsional deformation (i.e., it is displaced toward the *E* isomer), the situation is different. Again, we have located two very steep relaxation paths leading to the *Z* and *E* species. However, in this case, the relaxation path starting in the close vicinity of the decay point leads, rather counterintuitively, to the *Z* isomer. This means that even in the absence of kinetic energy decay at point D would lead back to the original reactant.

The analysis of the extreme decay points C and D indicates that different situations are possible. In certain cases the surface topography controls the reaction outcome and, ultimately, the reaction quantum yield. In other cases, such as the case of the decay point C, it is really a dynamical effect that determines the reaction outcome.

4. Conclusions

The photochemistry of the (*Z*)-pentadieniminium cation **1**, which is a model system for the chromophore of certain retinal binding proteins, has been studied with respect to the $Z \rightarrow E$ isomerization of the central double bond. We have been able to locate a low-lying intersection seam connecting the S_0 and S_1 potential energy surfaces spanning the entire range of twist angles from 0° to 180°. The fact that essentially no torsion is involved in the gradient difference and derivative coupling vectors proves that the torsional coordinate that dominates the reaction path in the excited state is part of the intersection space; this explains why the seam persists through all values of the central torsional angle of **1**.

Initial conditions for the trajectories were obtained using ground-state zero-point energy sampling, which provides an ensemble of Franck−Condon geometries. Despite the existence of a conical intersection for every point along the torsional coordinate, semiclassical trajectory calculations show that there is a preferred reaction channel. Only a limited range of twist angles, between 60° and 80°, lead to S_1-S_0 decay events. This is in line with MEP studies reported earlier in which the excited-state reaction path of **1** was found to connect with the ground state via a CI with a 70° twist angle. These findings support the idea that the motion toward the crossing section is determined by the structure of the excited-state PES rather than by the initial conditions—geometry and momenta—of the excited molecule. The zero-point energy in our molecular dynamics study is transferred mainly into modes orthogonal to the reaction coordinate (i.e., stretching modes); this energy is not sufficient to sample the whole $CI_{0°}-CI_{180°}$ intersection line, but only a limited segment near the $CI_{70°}$ minimum. Accordingly, motion along the reaction path is a good description of the photochemistry of the (*Z*)-pentadieniminium cation.

Further analysis of the sampled dynamics reveals that the photoreaction is nearly diabatic, with half of the trajectories decaying at an energy gap of less than 4 kcal mol^{-1}. Also, the reaction is extremely efficient, with a quantum yield higher than 80%. This strongly supports the idea that the wave packet is decaying in a way that recalls the classical Landau−Zeener model for nonadiabatic transitions. In this context the quantum yield—which is actually higher than the experimentally observed value for protonated retinal Schiff bases in solution and in a protein environment—would be the result of a high average velocity at the hopping event, which takes place only 50−80 fs after excitation. The calculations suggest that in **1** the branching ratio, i.e., the ratio between successful and nonsuccessful hopping events leading to the *E* and the *Z* products, respectively,

is mainly controlled by the dynamics and to a lesser extent by the PES. This is consistent with the ground-state relaxation path mappings presented in this study.

In our minimal retinal model study the rhodopsin protein environment has not been incorporated. However, it is now widely accepted that on the time scale studied in our dynamics intermolecular relaxation processes will only be of minor influence, since such processes progress in the picosecond rather than the femtosecond range. In a recent paper it was also possible to show that, from the point of view of the chromophore wave function, the interior of the protein cavity appears to be more similar to a gas-phase environment than to a solution environment.[29] Apart from the steric effects of the protein, which would produce different inital geometries, our gas-phase model provides a promising description for the ultrafast dynamics of *cis*−*trans* isomerizations in protonated Schiff bases.

Acknowledgment. Funds have been provided by the Università di Siena (Progetto di Ateneo 02/04), HFSP (Grant RG 0229/2000-M). A.M. is grateful for a grant provided. We also thank the Deutsche Forschungsgemeinschaft (DFG graduate college Struktur und Dynamik heterogener Systeme) and the European Union (MC Training Site Contract HPMT-CT-2000-00062) for financial support, and we thank CINECA for granted calculation time.

Supporting Information Available: (1) Discussion about the relationship between the excited-state reaction path and the intersection seam cross-section for the S_1 $E \rightarrow Z$ isomerization of **2** (comprising Figures S1−S3, Table S1, and Scheme S1) and (2) determination of lowest energy intersection points with a 0° (180°) $C_2-C_3-C_4-C_5$ torsion (comprising Figures S4−S6, Table S2, Figure S7 describing the geometrical changes in the $FC_{180°}-CI_{92°}$ excited-state reaction path and the $CI_{180°}-CI_{92°}$ intersection seam segment, and six tables containing the Cartesian coordinates for the CASSCF/6-31G*-optimized structures discussed in the text). This material is available free of charge via the Internet at http://pubs.acs.org.

References and Notes

(1) Bernardi, F.; Olivucci, M.; Robb, M. A. *Chem. Soc. Rev.* **1996**, 321−328.

(2) Atchity, G. J.; Xantheas, S. S.; Ruedenberg, K. *J. Chem. Phys.* **1991**, *95*, 1862.

(3) Robb, M. A.; Garavelli, M.; Olivucci, M.; Bernardi, F. In *Reviews in Computational Chemistry*; Lipkowitz, K. B., Boyd, D. B., Eds.; Wiley-VCH, John Wiley and Sons Inc.: New York, Chichester, U.K., 2000; pp 87−146.

(4) Garavelli, M.; Celani, P.; Bernardi, F.; Robb, M. A.; Olivucci, M. *J. Am. Chem. Soc.* **1997**, *119*, 6891−6901.

(5) Sanchez-Galvez, A.; Hunt, P.; Robb, M. A.; Olivucci, M.; Vreven, T.; Schlegel, H. B. *J. Am. Chem. Soc.* **2000**, *122*, 2911−2924.

(6) Boggio-Pasqua, M.; Bearpark, M. J.; Hunt, P. A.; Robb, M. A. *J. Am. Chem. Soc.* **2002**, *124* (7), 1456−1470.

(7) Ben-Nun, M.; Martinez, T. J. *Chem. Phys. Lett.* **1998**, *298*, 57−65.

(8) Migani, A.; Robb, M. A.; Olivucci, M. *J. Am. Chem. Soc.* **2003**, *125* (9), 2804−2808.

(9) Buss, V.; Weingart, O.; Sugihara, M. *Angew. Chem., Int.Ed.* **2000**, *39*, 2784−2786.

(10) Vreven, T.; Bernardi, F.; Garavelli, M.; Olivucci, M.; Robb, M. A.; Schlegel, H. B. *J. Am. Chem. Soc.* **1997**, *119*, 12687−12688.

(11) Millam, J. M.; Bakken, V.; Chen, W.; Hase, W. L.; Schlegel, H. B. *J. Chem. Phys.* **1999**, *111*, 3800−3805.

(12) Helgaker, T.; Uggerud, E.; Jensen, H. J. A. *Chem. Phys. Lett.* **1990**, *173*, 145−150.

(13) Tully, J. C.; Preston, R. K. *J. Chem. Phys.* **1971**, *55*, 562−572.

(14) Garavelli, M.; Page, C. S.; Celani, P.; Olivucci, M.; Schmid, W. E.; Trushin, S. A.; Fuss, W. *J. Phys. Chem. A* **2001**, *105*, 4458−4469.

(15) Sinicropi, A.; Migani, A.; Vico, L. D. *Photochem. Photobiol. Sci.* **2003**, *2*, 1250−1255.

(16) Hase, W. L. *Encyclopaedia of Computational Chemistry*; John-Wiley & Sons: 1998; pp 402−407.

(17) Frisch, M. J.; Trucks, G. W.; Schlegel, H. B.; Scuseria, G. E.; Robb, M. A.; Cheeseman, J. R.; Zakrzewski, V. G.; Montgomery, J. A., Jr.; Stratmann, R. E.; Burant, J. C.; Dapprich, S.; Millam, J. M.; Daniels, A. D.; Kudin, K. N.; Strain, M. C.; Farkas, O.; Tomasi, J.; Barone, V.; Cossi, M.; Cammi, R.; Mennucci, B.; Pomelli, C.; Adamo, C.; Clifford, S.; Ochterski, J.; Petersson, G. A.; Ayala, P. Y.; Cui, Q.; Morokuma, K.; Malick, D. K.; Rabuck, A. D.; Raghavachari, K.; Foresman, J. B.; Cioslowski, J.; Ortiz, J. V.; Baboul, A. G.; Stefanov, B. B.; Liu, G.; Liashenko, A.; Piskorz, P.; Komaromi, I.; Gomperts, R.; Martin, R. L.; Fox, D. J.; Keith, T.; Al-Laham, M. A.; Peng, C. Y.; Nanayakkara, A.; Gonzalez, C.; Challacombe, M.; Gill, P. M. W.; Johnson, B.; Chen, W.; Wong, M. W.; Andres, J. L.; Gonzalez, C.; Head-Gordon, M.; Replogle, E. S.; Pople, J. A. *Gaussian 98*; Gaussian, Inc.: Pittsburgh, PA, 1998.

(18) Frisch, M. J.; Trucks, G. W.; Schlegel, H. B.; Scuseria, G. E.; Robb, M. A.; Cheeseman, J. R.; Zakrzewski, V. G.; Montgomery, J. A., Jr.; Stratmann, R. E.; Burant, J. C.; Dapprich, S.; Millam, J. M.; Daniels, A. D.; Kudin, K. N.; Strain, M. C.; Farkas, O.; Tomasi, J.; Barone, V.; Mennucci, B.; Cossi, M.; Adamo, C.; Jaramillo, J.; Cammi, R.; Pomelli, C.; Ochterski, J.; Petersson, G. A.; Ayala, P. Y.; Morokuma, K.; Malick, D. K.; Rabuck, A. D.; Raghavachari, K.; Foresman, J. B.; Ortiz, J. V.; Cui, Q.; Baboul, A. G.; Clifford, S.; Cioslowski, J.; Stefanov, B. B.; Liu, G.; Liashenko, A.; Piskorz, P.; Komaromi, I.; Gomperts, R.; Martin, R. L.; Fox, D. J.; Keith, T.; Al-Laham, M. A.; Peng, C. Y.; Nanayakkara, A.; Challacombe, M.; Gill, P. M. W.; Johnson, B.; Chen, W.; Wong, M. W.; Andres, J. L.; Gonzalez, C.; Head-Gordon, M.; Replogle, E. S.; Pople, J. A. *Gaussian 99*; Gaussian, Inc.: Pittsburgh, PA, 2000.

(19) Celani, O.; Robb, M. A.; Garavelli, M.; Bernardi, F.; Olivucci, M. *Chem. Phys. Lett.* **1995**, *243*, 1.

(20) Bearpark, M. J.; Robb, M. A.; Schlegel, H. B. *Chem. Phys. Lett.* **1994**, *223*, 269.

(21) Chen, W.; Hase, W. L.; Schlegel, B. *Chem. Phys. Lett.* **1994**, *228*, 436−442.

(22) Paterson, M. J.; Hunt, P. A.; Robb, M. A.; Takahashi, O. *J. Phys. Chem. A* **2003**, *106* (44), 10494−10504.

(23) Blancafort, L.; Ogliaro, F.; Olivucci, M.; Robb, M. A.; Bearpark, M. J.; Sinicropi, A. In *Computational Methods in Photochemistry*; Kutateladze, A., Ed.; Marcel Dekker: New York, in press.

(24) Ben-Nun, M.; Martinez, T. *J. Chem. Phys.* **2000**, *259*, 237−248.

(25) Freedman, K. A.; Becker, R. S. *J. Am. Chem. Soc.* **1986**, *108*, 1245−1251.

(26) Kandori, H.; Shichida, Y.; Yoshizawa, T. *Biochemistry (Moscow)* **2001**, *66* (11), 1483−1498.

(27) Warshel, A.; Chu, Z. T. *J. Phys. Chem. B* **2001**, *105*, 9857−9871.

(28) Garavelli, M.; Celani, P.; Fato, M.; Bearpark, M. J.; Smith, B. R.; Olivucci, M.; Robb, M. A. *J. Phys. Chem. A* **1997**, *101*, 2023−2032.

(29) Ferre, N.; Olivucci, M. *J. Am. Chem. Soc.* **2002**, *125*, 6868−6869.